Macromolecules

Article

pubs.acs.org/Macromolecules

Formation Mechanism of High-Density, Flattened Polymer Nanolayers Adsorbed on Planar Solids

Naisheng Jiang,[†] Jun Shang,[†] Xiaoyu Di,[†] Maya K. Endoh,[†] and Tadanori Koga[†,‡,§,*]

[†]Department of Materials Science and Engineering, Stony Brook University, Stony Brook, New York 11794-2275, United States

[‡]Chemical and Molecular Engineering Program, Stony Brook University, Stony Brook, New York 11794-2275, United States

[§]Department of Chemistry, Stony Brook University, Stony Brook, New York 11794-3400, United States

Supporting Information

ABSTRACT: Thermal annealing is one of the most indispensable polymer fabrication processes and plays essential roles in controlling morphologies and properties of polymeric materials. We here report that thermal annealing also facilitates polymer adsorption from the melt on planar silicon (Si) substrates, resulting in the formation of a high-density polymer nanolayer with flattened chain confirmations. Three different homopolymers (polystyrene, poly(2-vinylpyridine), and poly(methyl methacrylate)), which have similar inherent stiffness and bulk glass transition temperature (T_g), but have different affinities with Si substrates, were chosen as models. Spin-cast films (~50 nm in thickness) with the three polymers were prepared on cleaned Si substrates and then placed in a vacuum oven set at a temperature far above the bulk T_g. In order to monitor the polymer adsorption process at the solid-polymer melt interface during thermal annealing, we used the protocol that combines vitrification of the annealed films (via rapid quench to room temperature) and subsequent intensive solvent leaching (to remove nonadsorbed chains). The detailed structures of the residual films (i.e., flattened layers with 2−3 nm in thickness) were characterized by using X-ray reflectivity and atomic force microscopy. As a result, we found that the film thicknesses of the flattened layers for the three different polymers increase as a power-law of annealing time before reaching the "quasiequilibrium" state where the film growth is saturated. We have also revealed that the final thickness of the flattened layer at the quasiequilibrium state increases with increasing the solid-segment interaction, while the kinetics becomes more sluggish. The observed formation kinetics corresponds to a "zipping-down" process of the transient flattened chains on planar solids in order to further increase the number of solid/segment points, which is the driving force for flattening so as to overcome the conformational entropy loss in the total free energy.

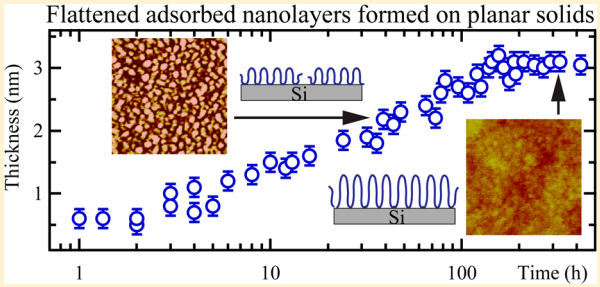

1. INTRODUCTION

A spin-coating process (i.e., a rapid solvent-cast process) is a well-established technique to prepare homogeneous polymer thin films on planar substrates in a well-controlled manner. But, it is also known that this rapid solvent evaporation process results in nonequilibrium stressed conformations of polymer chains on substrates and such residual stress causes film instability[1−3] and changes in properties of polymer thin films.[4−6] In order to achieve full relaxation of the residual stress and equilibration of the chain conformations, prolong thermal annealing (at temperatures far above the bulk T_g) compared to bulk reputation times[7] is typically required.[3,8,9] On the other hand, prolonged thermal annealing expedites polymer adsorption from the melt onto solid substrates.[10] On the basis of the established protocol combined thermal annealing at a temperature far above T_g and subsequent rinsing with a good solvent, several research groups have shown the formation of irreversibly adsorbed polymer layers with thickness of several nanometers to a few tens of nanometers even onto weakly attractive surfaces.[11−19] The vital points of such adsorbed layers (known as Guiselin brushes[20]) are to (i) create an "interphase" with the properties between those of the adsorbed layer and bulk even for weakly interactive systems[21−23] and (ii) control the structures,[24,25] dynamics[18,26] and other physical properties[27−32] of polymer thin films. Recently, our group has demonstrated that polystyrene (PS) adsorbed layers on planar Si substrates are composed of an inner higher density region (~2 nm in thickness regardless of molecular weights (M_w)) with a more flattened chain conformation and an outer bulk-like density region whose thickness increases with M_w.[19] Hereafter, we assign the inner high-density layer and outer bulk-like density layer as the "flattened layer" and "loosely adsorbed layer", respectively. It is postulated that this two-layer formation is attributed to piecemeal deposition with differential spreading dictated by the still-uncovered surface area, as reported in polymer adsorption from dilute solutions.[33−36] The formation of the flattened layer on planar substrates is consistent with the Brownian dynamic simulation results

Received: February 15, 2014
Revised: April 2, 2014
Published: April 8, 2014

   dx.doi.org/10.1021/ma5003485 | Macromolecules 2014, 47, 2682−2689

Table 1. Characteristics of the Polymers Used in the Study

polymer	M_w (kDa)	M_w/M_n	$T_{g,\,bulk}$ (°C)	surface tension (mJ/m^2) γ	γ_D	γ_P	γ_{ls} (mJ/m^2)[a]	l (nm)[b]
PS	50	1.04	100	40.6	34.5	6.1	5.6	0.9
	290	1.04						
	650	1.07						
PMMA	97	1.05	105	41.1	29.6	11.5	3	0.85
P2VP	200	1.5	98	[c]			strongest[50,51d]	0.9

[a]Interfacial energy. [b]Persistence length.[90] [c]No data available. [d]Strongest interactions among the three polymers according to the references.

reported by Linse and co-workers:[37] Flexible homopolymer adsorbed chains tend to orient their conformations parallel to the surface and form a compact, higher density layer relative to the bulk in equilibrium. The flattened chain conformation can be in principle drawn by a counterbalance between the conformational entropy of chains and the energy gain of attached segments to the surface in the total free energy.[19,38]

In this paper, we aim to understand the formation process of the flattened layer from the melt by distinguishing from that of the loosely adsorbed polymer layer on planar substrates. In contrast to irreversible adsorption from dilute polymer solutions, the kinetics from the melt is more sluggish and complicated due to chain entanglements, friction, and incomplete equilibration.[39,40] Yet, several recent dielectric spectroscopy studies reported by Napolitano and co-workers[31,41,42] showed that the growth of the polymer adsorbed layers (which should be composed of the flattened and loosely adsorbed layers, while they never clarified it) on planar solids exhibit power-law growth at the early stage of adsorption and gives way to a slower logarithmic growth before reaching the final chain conformations. This overall behavior is similar to irreversible polymer adsorption from dilute solution.[33−36,43,44] However, the kinetics of the inner two-layer formation is still untouched. Here, we use three different homopolymers, polystyrene (PS), poly(2-vinylpyridine) (P2VP), and poly(methyl methacrylate) (PMMA) as models since these polymers have similar inherent stiffness and bulk glass transition temperature (T_g), but different affinities with Si substrates. We have optimized the thermal annealing and solvent leaching conditions to extract the lone flatten layers on planar substrates. X-ray reflectivity and atomic force microscopy techniques allow detailed characterization of the flattened layers at the nanometer scale. A series of the experimental findings shed light on the importance of the polymer/substrate interactions in the final structures and formation kinetics of the flattened chains at the solid-polymer melt interface.

II. MATERIALS AND METHODS

II-1. Sample Preparation. PS, P2VP, and PMMA were purchased from Pressure Chemical Co., Polysciences Inc., and Scientific Polymer Products Inc., respectively. The characteristics are tabulated in Table 1. The polymers were dissolved in a good solvent (toluene (Sigma-Aldrich, HPLC grade, > 99.9%) for PS and PMMA, and dimethylformamide (DMF, Sigma-Aldrich, ACS reagent, > 99.8%) for P2VP) with polymer concentrations of about 2.5 wt %. Si substrates were cleaned by immersion in a hot piranha solution (i.e., a mixture of H_2SO_4 and H_2O_2 [*Caution!* A piranha solution *is highly corrosive upon contact with skin or eyes and is an explosion hazard when mixed with organic chemicals/materials; extreme care should be taken when handing it*]) for 30 min, and subsequently rinsed with deionized water thoroughly. Then, only for preparation of PS thin films, we used an aqueous solution of hydrogen fluoride (HF) to remove a native oxide layer on Si substrates. Hereafter, we assign hydrogen passivated Si substrates and Si without the HF treatment as H−Si and B−Si, respectively. It should be noted that a SiO_2 layer of about 1 nm in thickness was reproduced even just after HF etching due to atmospheric oxygen and moisture.[45] However, the surface tension (γ) of the H−Si is quite different (48.71 mJ/m^2 for the dispersion part (γ_d) and 3.98 mJ/m^2 for the polar part (γ_p)[46]) from that of the B−Si (γ_d = 25.8 mJ/m^2 and γ_p = 25.8 mJ/m^2[47]). As summarized in Table 1, the interfacial energy (γ_{ls}) between the polymer and the substrate were calculated based on the Owens−Wendt−Kaelble equation[48,49] with the respective surface tension. To prepare the final flattened layer, we reproduced the established protocol:[19] Approximately 50 nm-thick spin-cast films prepared on either H−Si or B−Si substrates were annealed at high temperatures (~T_g + 50 °C) for long time (typically several days) under vacuum below 10^{-3} Torr; the films were then leached in baths of a fresh good solvent at room temperature until the resultant film thickness remained constant. In the case of P2VP, the T_g of supported P2VP thin films is reported to increase significantly compared to the bulk value.[50,51] Hence, we chose further higher temperature (~T_g + 90 °C) as the annealing temperature. As will be discussed later, the leaching conditions used (type of a solvent, leaching time, leaching temperature etc.) should be optimized; otherwise we might end up with the formation along with the loosely adsorbed layers. This selective extraction of the two adsorbed layers is possible owing to the large difference in the desorption energy between the outer loosely adsorbed chains and the flattened chains, which is proportional to the number of segment-surface contacts.[52,53] We have also validated that the flattened layer is formed before the solvent leaching process (see Supporting Information). The resultant polymer flattened layers were dried in a vacuum oven at 150−190 °C, depending on the polymers, for 24 h to remove any excess solvent trapped in the films before further experiments.

II-2. X-ray Reflectivity (XR). XR experiments were performed under vacuum (approximately 10^{-4}−10^{-5} Torr) at the X10B and X20A beamlines of the National Synchrotron Light Source, Brookhaven National Laboratory. The specular reflectivity was measured as a function of the scattering vector in the direction perpendicular to the surface, $q_z = 4\pi[\sin\theta]/\lambda$, where θ is the incident angle and λ is the X-ray wavelength (λ = 0.087 nm at X10B and λ = 0.118 nm at X20A, which are equivalent to the X-ray energy of 14.2 and 10.5 keV, respectively). The XR data was fit by using a standard multilayer fitting routine for a dispersion value (δ in the X-ray refractive index) in conjunction with a Fourier transformation (FT) method, a powerful tool to obtain detailed structures for low X-ray contrast polymer multilayers.[54,55] In order to study the thermal stability of the flattened layers, we also performed high temperature XR under vacuum by using a custom-built vacuum furnace with Kapton windows. The films were first heated to high temperature (150−200 °C), and XR measurements were initiated from the cooling process at a temperature interval of 10 °C. Heating and recooling experiments were also performed to ensure reproducibility. At given temperatures, we stabilized the films for approximately 1 h before data collection.

II-3. Atomic Force Microscopy (AFM) Measurements. Surface morphologies of the flattened and loosely adsorbed layers were studied by using atomic force microscopy (AFM) (Bruker Bioscope Catalyst and Digital Nanoscope III). A standard tapping mode was conducted in air by using a cantilever with a spring constant of about 40 N/m and

dx.doi.org/10.1021/ma5003485 | Macromolecules 2014, 47, 2682−2689

a resonant frequency of about 300 kHz. The scan rate was 1.0 Hz with a scanning density of 256 or 512 lines per frame.

III. RESULTS AND DISCUSSION

III-1. Formation Kinetics: Loosely Adsorbed Chains vs Flattened Chains. Before moving into the main topics, it would be useful to describe the terminology to be used. Granick and co-workers pointed out that when the surface sticking energy per monomer reaches values of only a few k_BT, polymer relaxation times become so large that equilibrium adsorbed layers may not be attained even from dilute solutions.[34,56−62] In addition, Napolitano and Wübbenhorst proposed that polymer chains adsorbed from the melt on solid substrates reach only a "metastable" state with an extremely long relaxation time.[17] Hence, we define the final adsorbed layers, whose thickness remains unchanged against annealing time, as a "quasiequilibrium" state,[63] unless otherwise stated. In addition, we assign the entire adsorbed layer composed of the inner flattened chains and outer loosely adsorbed chains as an "interfacial sublayer".[64]

First, we aim to differentiate the formation kinetics of the lone flattened layer from the interfacial sublayer by using PS since the formation protocols for both layers have been established.[15,17,19,31,42] A monodisperse PS (weight-average molecular mass (M_w) = 290 kDa) was used for this purpose. For the formation of the interfacial sublayer, spin-cast PS films (~50 nm in thickness) prepared on H−Si substrates were annealed at 150 °C for up to 200 h and then solvent leached at minimum of 5 times in baths of fresh toluene at room temperature.[19] In the case of the flattened layer, we previously demonstrated that a further intensive leaching process (~120 days) with toluene at room temperature enables us to remove the outer loosely adsorbed layer preferentially.[19] However, as will be discussed below, we here adopted an alternative leaching process with chloroform at room temperature that allows us to more effectively uncover the lone flattened layer within a total leaching time of a couple of days. Here we show how the two different solvent leaching processes work to prepare the two different chain conformations on H−Si substrates. Figure 1 shows the XR profiles of the interfacial sublayer and the flattened PS layer at annealing time (t_{an}) of 100 h. The corresponding best fits (shown in the solid lines in Figure 1) to the XR data were obtained by using a three-layer (a Si substrate, a SiO_2 layer, and a PS layer) dispersion model for the flattened layer and a four-layer (a Si substrate, a SiO_2 layer, and two PS layers with different densities) for the interfacial sublayer, respectively (the inset of Figure 1). The choices of these layer models were determined by the corresponding FT profiles of the XR profiles and the details have been described elsewhere.[19] Note that the δ value of the bulk PS with the X-ray energy of 14.2 keV is $\delta_{bulk} = 1.14 \times 10^{-6}$. From independent XR measurements using a H−Si substrate, the thickness of the SiO_2 layer was determined to be 1.3 nm (2.4 nm for a bare B−Si layer). Hence, the XR results clearly show that the interfacial sublayer is composed of the inner higher-density layer (~15% higher than the bulk) and the outer bulk-like density layer, and the thickness of the lone flattened layer after the chloroform leaching is in good agreement with that of the inner high-density region of the interfacial sublayer. Hence, the results validate that we have successfully extracted the lone flattened layer by the chloroform rinsing. Note that the δ value of the lone flattened layer is smaller than that within the interfacial sublayer due to the empty (air) spaces of the film, as discussed below.

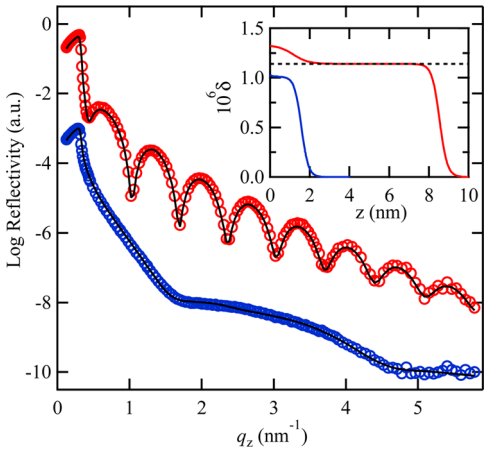

Figure 1. XR curves of the quasiequilibrium PS (M_w = 290 kDa) interfacial sublayer (red circles) and flattened layer (blue circles) at t_{an} = 100 h. The solid lines correspond to the best-fits to the data based on the dispersion (δ) profiles against the distance (z) from the SiO_2 surface shown in the inset: red line, the interfacial sublayer; blue line, the flattened layer. The dotted line in the inset corresponds to the δ value of bulk PS.

As shown in Figure 2a, the flattened layer has microscopic "textures" with the characteristic length of about 100 nm, while the surface of the interfacial sublayer is homogeneous (Figure 2b) at t_{an} = 100 h. As shown in Figure 2c, the average height of the surface textures from the SiO_2 surface is estimated to be about 3 nm, which is in reasonably agreement with the XR result. In order to estimate the surface coverage (ϕ_p) of the flattened polymer chains, we applied bearing area analysis using NanoScope Analysis software (version 1.40, Bruker). A bearing area gives a percentage of the surface above a critical threshold.

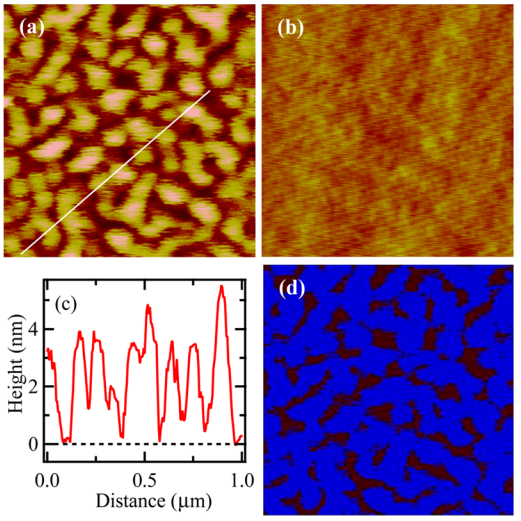

Figure 2. AFM height images of (a) the PS (M_w = 290 kDa) flattened layer surface and (b) interfacial sublayer surface at t_{an} = 100 h. The scan sizes and height scales of the images are 1 μm × 1 μm and 0−6 nm, respectively. The corresponding height profile along the white line in part a is plotted in part c. The dotted line corresponds to the SiO_2 surface. (d) Corresponding bearing area analysis result for the AFM image shown in part a. The areas occupied by the polymer (bearing areas) are colored in blue.

dx.doi.org/10.1021/ma5003485 | Macromolecules 2014, 47, 2682−2689

For this analysis, AFM height images were used and we set the critical threshold (i.e., the polymer/SiO_2 interface) to 0 nm. Figure 2d shows a representative bearing analysis result of the AFM image shown in Figure 2a. The ϕ_p value was estimated to be 75 ± 5% based on several AFM images at different spots of the film. Since the loosely adsorbed chains cover the substrate homogeneously at t_{an} = 100 h (Figure 2b), it is reasonable to suppose that the empty regions (~25%) of the flattened layer correspond to the sites where the loosely adsorbed chains grew and were then removed by the chloroform leaching. These results are consistent with a set of polymer adsorption experiments from dilute solutions reported by Granick and co-workers,[60,65] who proved that the flattened chain conformations have much higher fractions than the loosely adsorbed chains. This problem is similar to random sequential adsorption for colloids and proteins.[66−72] The present surface coverage of 75% is much larger than the "jamming limit" (54.7% of surface sites) predicted for rigid disks,[66] suggesting that flexible polymer chains can adsorb more effectively and compactly by taking advantage of their flexibility to accommodate the limited surface sites.

Figure 3 shows the thickness of the PS flattened layer (h_f) measured by XR against t_{an}. From the figure we can see the

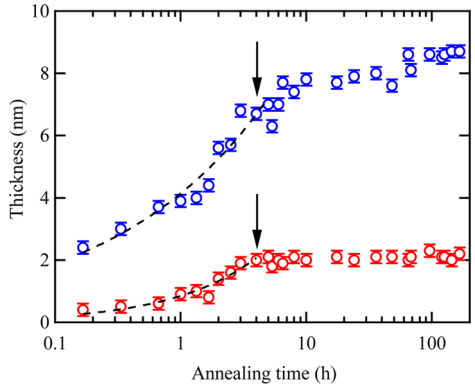

Figure 3. Growth of the PS (M_w = 290 kDa) interfacial sublayer (blue circles) and flattened layer (red circles) against t_{an} at 150 °C. The dotted lines correspond to the best-fits of the power-law growth described in the text. The crossover times from the power-law growth to logarithmic growth for the interfacial sublayer and from the power-law growth to the quasiequilibrium state for the flatten layer are indicated in the arrows.

flattened layer (red circles) exhibits a power-law growth ($h_f \propto t_{an}^{\alpha}$) with α = 0.50 ± 0.05 at the early stage of the kinetics and reached the quasiequilibrium conformation with the thickness of 2.1 nm after t_{an} > 4 h. Figure 3 also plots the time evolution of the thickness of the PS interfacial sublayer. We can see that the interfacial sublayer exhibits similar power-law growth with α = 0.36 ± 0.04 at the early stage kinetics, which is slower than that for the flattened layer due to the limited space issues, and there is a crossover time (t_c) at around 4 h, where the power-law behavior gives way to a slower logarithmic growth, followed by a plateau region at t_{an} > 96 h. The overall adsorption kinetics of the interfacial sublayer is in good agreement with previous experimental results on the adsorbed PS monolayers on Al substrates.[31,42] Interestingly, the crossover time (t_c = 4 h) for the interfacial sublayer is nearly equivalent to that of the flattened layer. Thus, the important conclusion is that the two different chain architectures emerge and grow independently on the solid surface.

III-2. The Effect of the Interactions on the Flattened Layer Formation. We next focus on the effect of the solid-segment interactions on the flattened layer formation. For this purpose, we compare P2VP, PMMA and PS flattened layers. Figure 4 shows the adsorption kinetics of these flattened layers.

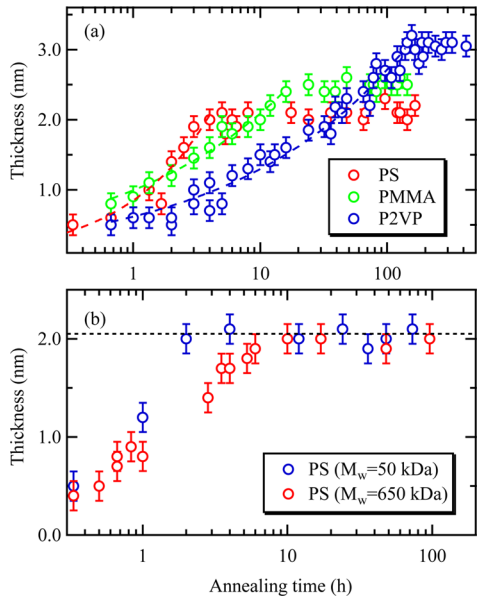

Figure 4. (a) Film thickness of the PS (M_w = 290 kDa), PMMA, and P2VP flattened layers against t_{an}. (b) Comparison of the growth of the two different PS (M_w =50 kDa and 650 kDa) flattened layers. The final thicknesses of the two PS flattened layers at the quasiequilibrium state (indicated in the dotted line) are equivalent.

The PMMA and P2VP flattened layers on B−Si substrates were extracted by intensive toluene and DMF leaching, respectively. From the figure we can see power-law growth of the P2VP and PMMA flattened layers before reaching the plateau regions (i.e., the quasiequilibrium state), but the exponents (~0.3) are slightly smaller than that of the PS flattened layer. In addition, it is likely that the final thickness and the t_c values increase with increasing the magnitude of the solid-segment interactions: P2VP > PMMA > PS (see, Table 1). To further consider the effect of the viscosity, which also affects the adsorption kinetics of entangled polymers, we investigated the adsorption kinetics of two other PS with different molecular weights (M_w = 50 kDa and 650 kDa). As shown in Figure 4(b), it was found that t_c increases with increasing M_w, while the final thickness remained constant, as previously reported.[19] However, the difference in t_c between the two PS flattened layers is at most 5 times, while the difference in the viscosity is more than 3 orders of magnitude based on the well-known relationship, $\eta \propto M_w^{3.4.7}$. Hence, the effect of the viscosity alone cannot explain the large difference (more than 2 orders of magnitude) in t_c between the PS (M_w = 290 kDa) and P2VP (M_w = 200 kDa). Hence, we may conclude that the magnitude of the interactions controls not only the final thickness but also the kinetics of the flattened layer formation. This can be qualitatively explained by simulation results that the number of polymer chains adsorbed on solids increase with increasing the solid-segment interaction.[37]

In order to further illuminate the difference in the adsorption kinetics among the three flattened layers, the detailed surface morphologies of the flattened layers were characterized by

dx.doi.org/10.1021/ma5003485 | Macromolecules 2014, 47, 2682−2689

AFM. Parts a and b of Figure 5 show the AFM height images of the PMMA and P2VP flattened layers after reaching the

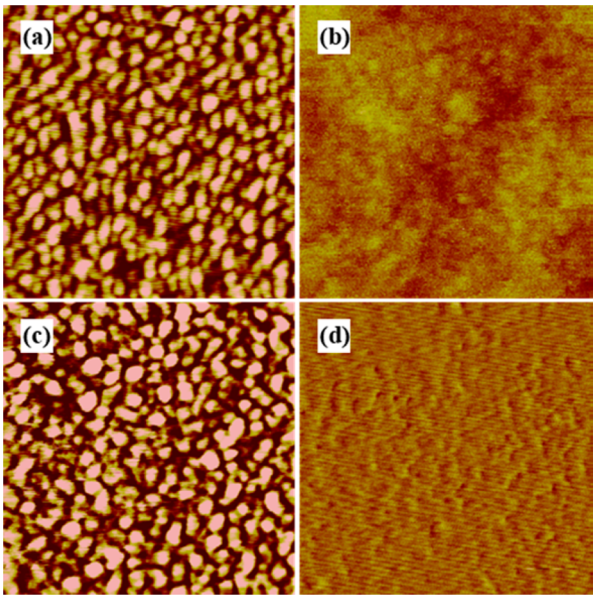

Figure 5. AFM height images of the (a) PMMA and (b) P2VP flattened layers at the quasiequilibrium state. The AFM phase image of the transient P2VP flattened layer at t_{an} = 65 h is shown in part c. A 50 nm-thick P2VP layer was directly spun cast on top of the transient flattened layer and then subject to thermal annealing at 190 °C for 168 h and subsequent DMF leaching. The surface morphology of the flattened layer resulted from the bilayer is shown in part d. The scan sizes and height scales of the images are 1 μm × 1 μm and 0−6 nm, respectively.

quasiequilibrium states. Hence, similar dimple structures are seen in the PMMA flattened layer and the surface coverage remains nearly identical (~75%) to that of the PS flattened layer (Figure 5a). On the other hand, we found that the P2VP flattened layer surface is reasonably uniform ($\phi_p \sim 90\%$) (Figure 5b). To further understand the effect of the solid-segment interactions on the dimple structures, we used polybutadiene (M_w = 100 kDa, M_w/M_n = 1.06, Polymer Source Inc.) that has a much weaker interaction with H−Si (γ_{ls} = 22.1 (mJ/m^2)). As a result, we found similar dimple structures with a surface coverage of ~70% and a relatively broad distribution of the characteristic lengths (30−140 nm) at the surface of the quasiequilibrium PB flattened layer (see Supporting Information). Hence, it is not conclusive yet whether the polymer/solid interaction is the main factor to control the size of the dimple structures, while the surface coverage tends to increase with increasing the interaction. On the other hand, it is noteworthy to point out that the dimple structures resemble of phase-separated structures (i.e., polymer-rich and polymer-poor regions) of end-grafted polymer brushes in a poor solvent regime.[73−81] We are currently studying whether the dimple structures are related to phase separation induced by the leaching process, i.e., immersing in the good solvent and subsequently exposing the flattened chains to air (a poor solvent).

IV. DISCUSSION

The polymer−polymer interactions become crucial when more polymers are adsorbed on solids. In the case of end-grafted polymer chains, as the grafting density increases, they will interact with one another and start to stretch in the direction normal to the surface due to excluded volume interactions between neighboring chains.[82] Here we may adopt the mechanism of end-grafting chains in order to explain the increase in the film thickness of the flattened layer. According to Aubouy and co-workers,[83] end-tethered polymer chains with large grafting density in polymer melts correspond to "dry (stretched) brushes", i.e., brush layers are substantially unpenetrated by matrix polymer chains, and the brush height proportionally increases with grafting density. As mentioned above, the irreversibly adsorbed polymer chains on solids are considered as the "Guiselin" brushes with many solid/segment contacts ($N^{1/2}$ contacts per chain).[20] Additionally, we have previously validated that the PS interfacial sublayer does not allow interpenetration of free polymer melt chains even at 170 °C ($\gg T_g$ of PS).[18] It is hence postulated that the inner flattened chains and the outer loosely adsorbed chains composed of the interfacial sublayer can be regarded as dry brushes. If this would be the case, the increases in the film thicknesses of the flattened layers shown in Figures 3 and 4 indicate the increases in the effective grafting density (i.e., the number of chain attachments per area in irreversible physisorption) of the flattened chains. The increase in the effective grafting density would be the driving force for flattening that is achieved by the energy gain of attached segments to the surface greater than the conformational entropy loss of the adsorbed chains in the total free energy.[19,38] At this point, it is not conclusive yet that the increase in the effective grafting density is correlated to the increase in ϕ_p.

The question arises: When is the formation of the flattened chains initiated on the substrate surface? According to previous simulation results, the time scale for early arriving polymer chains to lie flat on solids is only a few hundred nanoseconds,[37,84−87] which is way beyond our experimental time scale. In fact, we found the formation of a very thin PS adsorbed layer (less than 1 nm in thickness) resulted from spin-casting alone without subsequent thermal annealing, as previously reported.[15,17,31,42] Hence, we expect that the initial (nonequilibrium) flattened chains emerge under solution conditions rather than under melt conditions,[11] and the adsorption kinetics of the flattened layer at $t < t_c$ corresponds to a "collapse and zipping-down" process onto solids[52,53] and the succeeding relaxation and rearrangement of the flattened conformations toward their quasiequilibrium states in the melt.

On the other hand, as shown in Figure 3, diffusion-controlled adsorption of late arriving chains (i.e., the origin of the loosely adsorbed polymer chains) also takes place at $t < t_c$, but it is retarded due to screening by the flattened chains already present at the surface. As a consequence, the late arriving chains form bridges jointing up nearby empty sites (i.e., the loosely adsorbed polymer chains).[52] The competition between the zipping down of the flattened chains and the diffusion-controlled adsorption of the late coming chains continues until $t = t_c$ when the substrate surface is fully covered. At $t > t_c$, the zipping down of the flattened layer formation is over and a "reeling-in" process of the partially adsorbed (late arriving) chains[63] governs. This reeling-in process in the melt is more sluggish due to excluded-volume repulsion of the already existing adsorbed chains and chain entanglements with unadsorbed chains, resulting in the very slow logarithmic growth of the film thickness before achieving the final state (Figure 3). As a consequence, the resultant two chain

dx.doi.org/10.1021/ma5003485 | Macromolecules 2014, 47, 2682−2689

architectures composed of the interfacial sublayer is analogous to those formed via polymer adsorption from a dilute solution.[33−36,43,44]

In order to further understand the formation mechanism of the flattened layer, we studied the time evolution of the surface morphologies of the P2VP flattened layer by AFM. As shown in Figure 5c, we clarified that the transient P2VP flattened layer at t_{an} = 65 h and subsequent DMF leaching also shows dimple structures with h_f = 2.3 nm and ϕ_p ∼75% that are nearly identical to those of the PS and PMMA quasiequilibrium flattened layers. As discussed above, the empty spaces of the transient P2VP flattened layer should be the sites where the loosely adsorbed chains grow. Hence, owing to the very strong solid-segment interaction, it is likely that the loosely adsorbed P2VP chains can further collapse and zip down onto the substrate surface,[37,84] transforming into the quasiequilibrium flattened chains (Figure 5b). At the same time, this would suggest that the transient flattened chains are still able to move or slide in the lateral direction in order to accommodate the further zipping down chains. To verify this homogenization process of the flattened layer surface, we used the patchy P2VP flattened layer as a "substrate" for a spin-cast P2VP (50 nm-thick) film. The "bilayer" film of the bottom transient flattened layer and top spin-cast layer was then subject to high temperature annealing at 190 °C for 168 h, which is beyond t_c (= 96 h) for P2VP, and subsequent leaching with DMF. As shown in Figure 5d, the resultant P2VP flattened layer extracted from the annealed bilayer is found to be homogeneous and somewhat thicker (3.9 nm in thickness) than that of the quasiequilibrium P2VP flattened layer shown in Figure 5b (3.1 nm in thickness), possibly owing to a further increase in the effective grafting density. It should be noted that we confirmed that the heterogeneous surfaces of the PS and PMMA quasiequilibrium flattened layers shown in Figures 2a and 5a remain nearly unchanged even after similar bilayer experiments.

Finally, we show the thermal stability of the quasiequilibrium flattened layers. On the basis of high temperature XR experiments, we found that the quasiequilibrium P2VP flattened layer shows no significant changes in the thickness up to 200 °C (Figure 6). If we use the same definition of T_g as bulk (i.e., a change in a slope in a plot of specific volume against temperature[88]), the XR data indicates that there is no T_g of the P2VP quasiequilibrium flattened layer up to 200 °C, which is far above the bulk T_g (= 98 °C). The same conclusion can be drawn for the PS and PMMA quasiequilibrium flattened layers (Figure 6) as well as the transient P2VP flattened layer at t_{an} = 65 h. These findings may be consistent with previous differential scanning calorimetry experiments: No evidence of T_g of intercalated PS chains confined between clay particles within the domain spacing of 3 nm.[89] Hence, the long-range segmental mobility is entirely restricted on the solid surface, while the flattened chains (at least at the transient state) are still able to move laterally, as discussed above. Further experiments on the global chain dynamics of the flattened chains deserve future work.

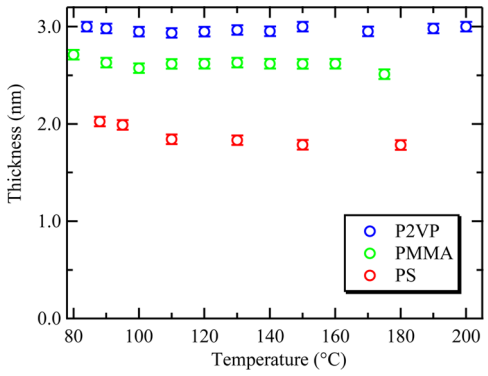

Figure 6. Film thicknesses of the three polymer flattened layers against temperature determined by the in situ XR measurements. The XR data was collected during the cooling process and heating processes, and we confirmed that all the temperature dependences of the film thicknesses are independent of the thermal processes.

V. CONCLUSION

We have revealed the effects of the solid/segment interactions on the formation of the high-density polymer flattened layers on planar Si substrates via thermal annealing of spin-cast polymer thin films. PS, P2VP, and PMMA homopolymers that have nearly identical stiffness and bulk T_g were chosen as models. The optimization of the thermal annealing and subsequent solvent leaching processes allowed us to unveil the lone flattened layer separately from the loosely adsorbed layer formed at the polymer melt/substrate interface simultaneously. X-ray reflectivity experiments have elucidated that the time growth of the flattened layers composed of the three different polymers exhibit similar power-law growth before reaching the quasiequilibrium state. Since the initial flattened chains are expected to be formed under solution conditions rather than under melt conditions,[11,37,84−87] the adsorption kinetics corresponds to the collapse and zipping-down process of the nonequilibrium flattened chains toward the quasiequilibrium state in the melt. The increase in the film thickness indicates that the transient flattened chains prefer to increase attaching points to the substrate so as to overcome the conformational entropy loss at the polymer melt-solid interface.[19,38] It was also found that as the solid-segment interaction becomes stronger, the thickness of the quasiequilibrium flattened layer increases, while the quasiequilibrium process becomes more sluggish. We are currently investigating the effect of chain stiffness, another crucial factor to control the adsorption kinetics,[87] on the formation process of the flattened layer. The details will be published elsewhere.

■ ASSOCIATED CONTENT

Supporting Information

AFM image of the quasiequilibrium PB flattened layer and clarification of the formation of the flattened layer before solvent leaching. This material is available free of charge via the Internet at http://pubs.acs.org.

■ AUTHOR INFORMATION

Corresponding Author

*(T.K.) E-mail: tadanori.koga@stonybrook.edu.

Notes

The authors declare no competing financial interest.

■ ACKNOWLEDGMENTS

We acknowledge Dongcui Li and the Bio-Imaging Center at the Delaware Biotechnology Institute (DBI) for partial AFM experiments. We also thank Steve Bennett and Jean Jordan-Sweet for the XR measurements. T.K. acknowledges partial financial support from NSF Grants (CMMI-084626 and

CMMI-1332499). Use of the National Synchrotron Light Source was supported by the U.S. Department of Energy, Office of Science, Office of Basic Energy Sciences, under Contract No. DE-AC02-98CH10886.

REFERENCES

(1) Richardson, H.; Carelli, C.; Keddie, J. L.; Sferrazza, M. *Eur. Phys. J. E* **2003**, *12*, 437−440.
(2) Reiter, G.; Hamieh, M.; Damman, P.; Sclavons, S.; Gabriele, S.; Vilmin, T.; Raphael, E. *Nat. Mater.* **2005**, *4*, 754−758.
(3) Damman, P.; Gabriele, S.; Coppée, S.; Desprez, S.; Villers, D.; Vilmin, T.; Raphaël, E.; Hamieh, M.; Al Akhrass, S.; Reiter, G. *Phys. Rev. Lett.* **2007**, *99*, 036101.
(4) Ziebert, F.; Raphael, E. *Phys. Rev. E* **2009**, *79*, 031605.
(5) Thomas, K. R.; Chenneviere, A.; Reiter, G.; Steiner, U. *Phys. Rev. E* **2011**, *83*, 021804.
(6) Barbero, D. R.; Steiner, U. *Phys. Rev. Lett.* **2009**, *102*, 248303.
(7) Doi, M.; Edwards, S. F. *The Theory of Polymer Dynamics*. Oxford Science: Oxford, U.K., 1986.
(8) Thomas, K. R.; Chenneviere, A.; Reiter, G.; Steiner, U. *Phys. Rev. E* **2011**, *83*, 021804.
(9) Chung, J. Y.; Chastek, T. Q.; Fasolka, M. J.; Ro, H. W.; Stafford, C. M. *ACS Nano* **2009**, *3*, 844−852.
(10) Fleer, G. J.; Cohen Stuart, M. A.; Scheutjens, J. M. H. M.; Cosgrove, T.; Vincent, B. *Polymers at Interfaces*; Chapman and Hall: London, 1993.
(11) Durning, C. J.; O'Shaughness, B.; Sawhney, U.; Nguyen, D.; Majewski, J.; Smith, G. S. *Macromolecules* **1999**, *32*, 6772−6781.
(12) Napolitano, S.; Prevosto, D.; Lucchesi, M.; Pingue, P.; D'Acunto, M.; Rolla, P. *Langmuir* **2007**, *23*, 2103−2109.
(13) Napolitano, S.; Wübbenhorst, M. *J. Phys. Chem. B* **2007**, *111*, 9197−9199.
(14) Napolitano, S.; Lupascu, V.; Wubbenhorst, M. *Macromolecules* **2008**, *41*, 1061−1063.
(15) Fujii, Y.; Yang, Z. H.; Leach, J.; Atarashi, H.; Tanaka, K.; Tsui, O. K. C. *Macromolecules* **2009**, *42*, 7418−7422.
(16) Napolitano, S.; Pilleri, A.; Rolla, P.; Wübbenhorst, M. *ACS Nano* **2010**, *4*, 841−848.
(17) Napolitano, S.; Wubbenhorst, M. *Nat. Commun.* **2011**, *2*, 260.
(18) Koga, T.; Jiang, N.; Gin, P.; Endoh, M. K.; Narayanan, S.; Lurio, L. B.; Sinha, S. K. *Phys. Rev. Lett.* **2011**, *107*, 225901.
(19) Gin, P.; Jiang, N.; Liang, C.; Taniguchi, T.; Akgun, B.; Satija, S. K.; Endoh, M. K.; Koga, T. *Phys. Rev. Lett.* **2012**, *109*, 265501.
(20) Guiselin, O. *Europhys. Lett.* **1992**, *17*, 225−230.
(21) Wallace, W. E.; van Zanten, J. H.; Wu, W. L. *Phys. Rev. E* **1995**, *52*, R3329−3332.
(22) van Zanten, J. H.; Wallace, W. E.; Wu, W. L. *Phys. Rev. E* **1996**, *53*, R2053−2056.
(23) Zhang, Y.; Ge, S.; Tang, B.; Koga, T.; Rafailovich, M. H.; Sokolov, J. C.; Peiffer, D. G.; Li, Z.; Dias, A. J.; McElrath, K. O.; Lin, M. Y.; Satija, S. K.; Urquhart, S. G.; Ade, H.; Nguyen, D. *Macromolecules* **2001**, *34*, 7056−7065.
(24) Asada, M.; Jiang, N.; Sendogdular, L.; Gin, P.; Wang, Y.; Endoh, M. K.; Koga, T.; Fukuto, M.; Schultz, D.; Lee, M.; Li, X.; Wang, J.; Kikuchi, M.; Takahara, A. *Macromolecules* **2012**, *45*, 7098−7106.
(25) Vanroy, B.; Wübbenhorst, M.; Napolitano, S. *ACS Macro Lett.* **2013**, *2*, 168−172.
(26) Zheng, X.; Rafailovich, M. H.; Sokolov, J.; Strzhemechny, Y.; Schwarz, S. A.; Sauer, B. B.; Rubinstein, M. *Phys. Rev. Lett.* **1997**, *79*, 241−244.
(27) Hu, H. W.; Granick, S. *Science* **1992**, *258*, 1339.
(28) Orts, W. J.; Vanzanten, J. H.; Wu, W. L.; Satija, S. K. *Phys. Rev. Lett.* **1993**, *71*, 867−870.
(29) Zheng, X.; Rafailovich, M. H.; Sokolov, J.; Strzhemechny, Y.; Schwarz, S. A.; Sauer, B. B.; Rubinstein, M. *Phys. Rev. Lett.* **1997**, *79*, 241−244.
(30) Napolitano, S.; Wubbenhorst, M. *Nat. Commun.* **2011**, 2.
(31) Napolitano, S.; Rotella, C.; Wübbenhorst, M. *ACS Macro Lett.* **2012**, *1*, 1189−1193.
(32) Labahn, D.; Mix, R.; Schönhals, A. *Phys. Rev. E* **2009**, *79*, 011801.
(33) Johnson, H. E.; Granick, S. *Science* **1992**, *255*, 966−968.
(34) Schneider, H. M.; Frantz, P.; Granick, S. *Langmuir* **1996**, *12*, 994−996.
(35) Soga, I.; Granick, S. *Langmuir* **1998**, *14*, 4266−4271.
(36) Douglas, J. F.; Johnson, H. E.; Granick, S. *Science* **1993**, *262*, 2010−2012.
(37) Linse, P.; Källrot, N. *Macromolecules* **2010**, *43*, 2054−2068.
(38) Schuetjens, M. H. M.; Fleer, G. J. *J. Phys. Chem.* **1980**, *84*, 178−190.
(39) Granick, S. *Eur. Phys. J. E* **2002**, *9*, 421−424.
(40) Santore, M. M. *Curr. Opin. Colloid Interface Sci.* **2005**, *10*, 176−183.
(41) Napolitano, S.; Capponi, S.; Vanroy, B. *Eur. Phys. J. E* **2013**, *36*, 1−37.
(42) Rotella, C.; Napolitano, S.; Vandendriessche, S.; Valev, V. K.; Verbiest, T.; Larkowska, M.; Kucharski, S.; Wubbenhorst, M. *Langmuir* **2011**, *27*, 13533−13538.
(43) Fu, Z. L.; Santore, M. *Macromolecules* **1999**, *32*, 1939−1948.
(44) Fu, Z.; Santore, M. M. *Langmuir* **1997**, *13*, 5779−5781.
(45) Shin, K.; Hu, X.; Zheng, X.; Rafailovich, M. H.; Sokolov, J.; Zaitsev, V.; Schwarz, S. A. *Macromolecules* **2001**, *34*, 4993−4998.
(46) Wang, Y.; Rafailovich, M.; Sokolov, J.; Gersappe, D.; Araki, T.; Zou, Y.; Kilcoyne, A. D. L.; Ade, H.; Marom, G.; Lustiger, A. *Phys. Rev. Lett.* **2006**, *96*, 028303.
(47) Kawai, A.; Kawakami, J.; Sasazaki, H. *J. Photopolym. Sci. Technol.* **2008**, *21*, 739−740.
(48) Israelachvili, J. N. *Intermolecular and surface forces*, revised third ed.; Academic Press: San Diego, CA, 2011.
(49) Kwok, D. Y.; Neumann, A. W. *Adv. Colloid Interface Sci.* **1999**, *81*, 167−249.
(50) vanZanten, J. H.; Wallace, W. E.; Wu, W. L. *Phys. Rev. E* **1996**, *53*, R2053−R2056.
(51) Roth, C. B.; McNerny, K. L.; Jager, W. F.; Torkelson, J. M. *Macromolecules* **2007**, *40*, 2568−2574.
(52) O'Shaughnessy, B.; Vavylonis, D. *Eur. Phys. J. E* **2003**, *11*, 213−230.
(53) O'Shaughnessy, B.; Vavylonis, D. *Phys. Rev. Lett.* **2003**, *90*, 056103.
(54) Seeck, O. H.; Kaendler, I. D.; Tolan, M.; Shin, K.; Rafailovich, M. H.; Sokolov, J.; Kolb, R. *Appl. Phys. Lett.* **2000**, *76*, 2713−2715.
(55) Koga, T.; Seo, Y. S.; Jerome, J. L.; Ge, S.; Rafailovich, M. H.; Sokolov, J. C.; Chu, B.; Seeck, O. H.; Tolan, M.; Kolb, R. *Appl. Phys. Lett.* **2003**, *83*, 4309−4311.
(56) Johnson, H. E.; Granick, S. *Macromolecules* **1990**, *23*, 3367−3374.
(57) Frantz, P.; Granick, S. *Phys. Rev. Lett.* **1991**, *66*, 899−902.
(58) Frantz, P.; Granick, S. *Macromolecules* **1994**, *27*, 2553−2558.
(59) Frantz, P.; Granick, S. *Macromolecules* **1995**, *28*, 6915−6925.
(60) Douglas, J. F.; Schneider, H. M.; Frantz, P.; Lipman, R.; Granick, S. *J. Phys.: Condens. Matter* **1997**, *9*, 7699−7718.
(61) Soga, I.; Granick, S. *Macromolecules* **1998**, *31*, 5450−5455.
(62) Zhao, J.; Granick, S. *Macromolecules* **2007**, *40*, 1243−1247.
(63) Zajac, R.; Chakrabarti, A. *Phys. Rev. E* **1995**, *52*, 6536−6549.
(64) Buenviaje, C.; Ge, S. R.; Rafailovich, M.; Sokolov, J.; Drake, J. M.; Overney, R. M. *Langmuir* **1999**, *15*, 6446−6450.
(65) Schneider, H. M.; Granick, S. *Macromolecules* **1992**, *25*, 5054−5059.
(66) Feder, J.; Giaever, I. *J. Colloid Interface Sci.* **1980**, *78*, 144−154.
(67) Onoda, G. Y.; Liniger, E. G. *Phys. Rev. A* **1986**, *33*, 715−716.
(68) Adamczyk, Z.; Siwek, B.; Zembala, M. *J. Colloid Interface Sci.* **1992**, *151*, 351−369.
(69) Ramsden, J. J. *J. Stat. Phys.* **1993**, *73*, 853−877.
(70) Ramsden, J. J. *Phys. Rev. Lett.* **1993**, *71*, 295−298.
(71) Adamczyk, Z.; Siwek, B.; Zembala, M.; Belouschek, P. *Adv. Colloid Interface Sci.* **1994**, *48*, 151−280.

(72) Van Tassel, P. R.; Viot, P.; Tarjus, G.; Talbot, J. *J. Chem. Phys.* **1994**, *101*, 7064−7073.
(73) Lai, P. Y.; Binder, K. *J. Chem. Phys.* **1992**, *97*, 586−595.
(74) Grest, G. S.; Murat, M. *Macromolecules* **1993**, *26*, 3108−3117.
(75) O'shea, S.; Welland, M.; Rayment, T. *Langmuir* **1993**, *9*, 1826−1835.
(76) Yeung, C.; Balazs, A. C.; Jasnow, D. *Macromolecules* **1993**, *26*, 1914−1921.
(77) Zhao, W.; Krausch, G.; Rafailovich, M.; Sokolov, J. *Macromolecules* **1994**, *27*, 2933−2935.
(78) Choi, B. C.; Choi, S.; Leckband, D. E. *Langmuir* **2013**, *29*, 5841−5850.
(79) Ishida, N.; Biggs, S. *Macromolecules* **2010**, *43*, 7269−7276.
(80) Ishida, N.; Biggs, S. *Langmuir* **2007**, *23*, 11083−11088.
(81) Carignano, M. A.; Szleifer, I. *J. Chem. Phys.* **1994**, *100*, 3210−3223.
(82) Jones, R. A.; Richards, R. W. *Polymers at Surfaces and Interfaces*. Cambridge University Press: Cambridge, U.K., 1999.
(83) Aubouy, M.; Fredrickson, G. H.; Pincus, P.; Raphaeel, E. *Macromolecules* **1995**, *28*, 2979−2981.
(84) Linse, P. *Soft Matter* **2012**, *8*, 5140−5150.
(85) Källrot, N.; Linse, P. *J. Phys. Chem. B* **2010**, *114*, 3741−3753.
(86) Källrot, N.; Dahlqvist, M.; Linse, P. *Macromolecules* **2009**, *42*, 3641−3649.
(87) Källrot, N.; Linse, P. *Macromolecules* **2007**, *40*, 4669−4679.
(88) Kovacs, A. J. *Adv. Polym. Sci.* **1964**, *3*, 394−508.
(89) Li, Y.; Ishida, H. *Macromolecules* **2005**, *38*, 6513−6519.
(90) *Polymer Handbook*, 4th ed. John Wiley & Sons, Inc.: New York, 1999.